# Impact of Tunnel Induced Stress Redistribution on Hydraulic Conductivity in Fractured Rocks

Quentin Courtois, Caroline Darcel, Romain Le Goc, Philippe Davy, Diego Mas Ivars, Eric Sykes

*International Society for Rock Mechanics and Rock Engineering*
*Norwegian Group for Rock Mechanics*

*ISRM International Symposium*
*Eurock 2025 – Expanding the Underground Space*
*Trondheim, Norway, 16-20 June*
*ISBN 978-82-8208-079-8*

# Impact of Tunnel Induced Stress Redistribution on Hydraulic Conductivity in Fractured Rocks

**Q. Courtois**[1], **C. Darcel**[1], **R. Le Goc**[1], **P. Davy**[2], **D. Mas Ivars**[3,4] **and E. Sykes**[5]

[1] Itasca Consultants S.A.S, France
[2] Géosciences Rennes, UMR 6118, Rennes University, France
[3] Swedish Nuclear Fuel and Waste Management Company (SKB), Solna, Sweden
[4] Division of Soil and Rock Mechanics, Department of Civil and Architectural Engineering, KTH Royal Institute of Technology, Sweden
[5] Nuclear Waste Management Organization (NWMO), Canada

## Abstract

Understanding the hydro-mechanical response of a crystalline rock mass to excavation is of critical importance to the safety assessment of underground nuclear waste disposal. This study analyzes the effect of tunnel-induced stress redistribution on the hydromechanical properties of fractured rocks, with a particular emphasis on fracture aperture, transmissivity and hydraulic conductivity.

The methodology involves the coupling of geomechanical (3DEC) and hydrogeological (DFN.lab) modeling software to study the complex interactions within fractured rock masses. The stress distributions are calculated using 3DEC, considering both the presence of the tunnel and the fractured rock mass. The computed stresses serve as input for DFN.lab, which calculates fracture transmissivities based on an empirical stress-transmissivity relationship. These fracture transmissivities are used to estimate upscaled hydraulic conductivities in various directions around the tunnel and at different scales.

One scenario is investigated, with consideration given to either solely the stress state induced by the tunnel or the combined stress state resulting from both the tunnel and the fractures. This approach accounts for interactions between fractures and subsequent stress fluctuations. The results indicate that tunnel excavation does not result in a significant increase in hydraulic conductivity. The results emphasize the influence of fracture orientation, connectivity and the orientation of the largest fractures on flow and stress variations. These factors highlight the sensitivity of model results to DFN realization and emphasize the need for detailed variability analyses. In addition, assumptions regarding fracture openness, particularly in the vicinity of the excavation zone, may need to be refined to accurately capture excavation-induced effects. This work contributes to the understanding of the hydromechanical response of fractured media to excavation and provides a framework for assessing site-specific conditions in underground engineering projects.

## Keywords

DFN, Geomechanics, Hydrogeology, Numerical modelling, Transmissivity-stress

ISRM

NBG

# 1 Introduction

The evaluation of the hydraulic properties in crystalline rocks is of critical importance for deep underground nuclear waste disposals. In these geological environments, fluid flow typically occurs only through the network of connected and transmissive fractures, while the rock matrix is impervious. Under undisturbed conditions, coupled processes are involved and in situ mechanical stresses are known to affect fracture aperture and transmissivity and hence potentially the rock mass equivalent hydraulic conductivity (Rutqvist & Stephansson, 2003; Tsang, 2024). During the construction of a repository and excavation of tunnels, the in-situ stress conditions will change, at least in the vicinity of the excavations, and may cause variations of the hydraulic properties (Jaeger et al., 2007).

The purpose of this study is to evaluate the effect of tunnel induced stress redistribution at depth on the hydraulic conductivity of the surrounding fractured rock mass. The latter is modeled as a rock into which the heterogeneities are the fracture system represented as a Discrete Fracture Network. The rock matrix around the fractures is assumed to be impermeable and the fluid flow through the rock mass occurs only within the fractures when they form connected pathways between hydraulically active boundary conditions. The hydromechanical coupling term is defined in the fracture stress-transmissivity law. In-situ stresses, resulting from geomechanical simulation, are calculated before and after tunnel excavation and are used as the input to the fracture transmissivity law. While the approach developed is general, it is only applied here under specific fracturing conditions that are close to the ones found at a depth of about 450 m at the Forsmark site in Sweden and for excavation dimensions typical of the tunnel dimensions found in a future deep geological repository.

# 2 Models and parameters

The rock mass is viewed as an initially homogeneous, impermeable and isotropic rock matrix into which a Discrete Fracture Network is embedded. The mechanical properties of both the rock matrix and the fractures are recalled in Table 2 and the hydraulic properties of the fractures are defined by the transmissivity law given in eq. 1.

The DFN model, at the depth of 450 m at the Forsmark site, is based on observations and interpretations derived from the site investigations and Site Descriptive Modeling phases (Fox et al., 2007; Olofsson et al., 2007; Darcel et al., 2009) led by SKB, the company in charge of the Deep Geological Repository (DGR) in Sweden. The modeling steps are in line with the methodology proposed in Selroos et al, 2022 and the resulting DFN model was recently used in (Davy et al 2023; Darcel et al 2024). The DFN model includes: (1) the Geo-DFN to represent all the fractures, regardless of their hydromechanical properties; (2) the Open-DFN is the subset of the Geo-DFN that contains only transmissive fractures; and (3) the Hydro-DFN includes only hydraulically connected open fractures with assigned transmissivities. In the present case, about 21 % of the total surface of fracture in the DFN is open (while the rest is sealed), as observed in core log data (Follin et al., 2014). In addition to this, the proportion of open fractures is assumed to increase with the fracture size (Davy et al., 2023). Both the Geo and the Open DFN follow a double power-law model (the scaling exponent is -4, respectively -3, for fractures larger, respectively smaller than the transition size $l_c$ (Figure 1a), consistent with the genetic DFN after (Davy et al., 2013). The transition scale $l_c$ is equal to 27m in the Open-DFN model. The fracture intensity of the Open-DFN model for fracture larger than 76 cm is 0.416 $m^2/m^3$. The fractures are mainly distributed in 4 families, 3 sub-vertical and one horizontal (Figure 1b). The principal stresses directions and average intensities at the target depth (Martin, 2007) are recalled in (Table 1). Both the maximum and intermediate principal stress are horizontal and the minimum one is vertical.

Under these conditions, future deposition tunnels will be horizontal and oriented in the direction of $\sigma_H$. The access, or transport, tunnels will be perpendicular to them (Figure 1c). The geomechanical and stress model focuses on a deposition tunnel, where the effects of excavation are to be assessed, and stress calculations to be performed. The domain extent of the geomechanical model is sketched in Figure 1a. It is oriented such that the local *y*-axis is aligned with the tunnel axis and direction of $\sigma_H$, the $x$ axis parallel to the minimum horizontal stress ($\sigma_h$) and the $z$ axis vertical. The domain size is 30 m, assuming that the excavation induced stress perturbation will not go beyond that distance.

*a*) *b*) *c*)

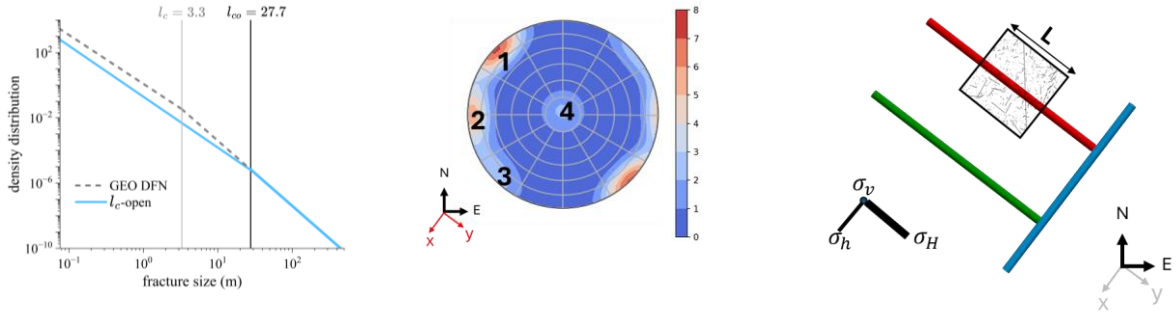


Figure 1.*a)* Fracture size density distribution for the Geo-DFN and Open-DFN models. The critical sizes for the transition between the two power-laws ($l_c$ for Geo-DFN and $l_{co}$ for Open-DFN) are highlighted. *b)* Stereographic view (equal area, lower hemisphere) of fracture orientations. The Fisher contour distribution (equal area, 1% circle size) is shown. *c)* Top view of the repository layout with 2 deposition and 1 transport tunnels and geomechanical domain with the DFN traces. The geographical and local axes of the domain are emphasized.

**Table 1. In-situ stress field at target depth.**

| $\sigma_H$ trend (°) | $\sigma_H$ (MPa) | $\sigma_h$ (MPa) | $\sigma_v$ (MPa) |
|---|---|---|---|
| 145 | 38.7 | 20.4 | 10.6 |

The fracture hydraulic aperture ($e_h$) law is given in (eq. 1) below, after Liu et al. (2004):

$$e_h = e_{hr} + (e_{max} - e_{hr}) \cdot \exp(-\sigma_n/\sigma_c) \quad (1)$$

with $e_h$ (m) the fracture hydraulic aperture, $\sigma_n$ the fracture average normal stress, $e_{hr}$ the fracture residual aperture (m), $e_{max}$ the fracture maximum aperture (m) and $\sigma_c$ a correlation term (Pa). The fracture transmissivity $T$ (m²/s) and hydraulic aperture are related by the classic cubic law (eq. 2) from (Snow, 1969):

$$T = \frac{\rho g}{12\mu} e_h^3 \quad (2)$$

where $\rho$ is the density of water (kg/m$^3$), $g$ is the acceleration of gravity (m²/s) and $\mu$ is the water dynamic viscosity (Pa.s).

# 3 Numerical implementation

First, a DFN realization is generated using DFN.lab (Le Goc et al., 2019). The DFN is next imported in a 3DEC (Itasca, 2024) model. Stresses are computed with the 3DEC model. For each fracture of the DFN, average normal and shear shear stresses are then derived and returned as to DFN.lab. Finally, transmissivities are calculated for each fracture from eq. 1 and 2, and fluid flow simulations are performed.

## 3.1 Geomechanical model

The geomechanical model is developed in 3DEC. It consists of an isotropic elastic matrix into which fractures are embedded. The fracture mechanical model is a Mohr-Coulomb model. The mechanical parameters are recalled in Table 2. Due to computational limitations (simulation time and mesh size), only a fraction of the DFN is explicitly imported into the 3DEC mesh (explicit fractures). The largest fractures are selected to be explicitly represented, regardless of their orientation, on the assumption that they have the largest potential effect on the stresses. The remaining fractures are only used to sample the stress field at the end of the simulation (implicit fractures), but do not affect the geomechanical behavior or the stress field.

During the geomechanical simulations, no reactivation of sealed fracture and no damage are allowed. The geomechanical domain is cubic and centered around a deposition tunnel (Figure 1c).

**Table 2. Fracture Mohr-Coulomb model parameters.**

| | | Value |
|---|---|---|
| Intact Rock | Young's Modulus (GPa) | 76 |
| | Poisson's ratio (-) | 0.25 |
| Fracture | Cohesion (MPa) | 0.3 |
| | Friction angle (°) | 35 |
| | Normal stiffness (GPa/m) | 656 |
| | Shear stiffness (GPa/m) | 34 |
| | Tensile strength (MPa) | 0 |
| | Dilation angle (°) | 5 |

The geomechanical modelling and stress computation is conducted in two main steps. First the normal stresses applying at the model domain boundaries are progressively increased during solving cycles, until target values are reached at the external faces of the model (maximum horizontal stress in the direction $y$, minimum horizontal stress in the direction $x$ and minimum vertical principal stress in the direction $z$, see Table 1). This is done with velocity boundary conditions (velocity component normal to each face of the model) combined with a servo control. Once the target stress values are reached the velocities vanish to zero and a first equilibrium is reached. At this stage, the in-situ stresses result from the external constraints combine with the stress fluctuations (Lavoine et al., 2024) induced by the fractures themselves. In the second step of the simulation, the tunnel is excavated at once and the model is cycled until equilibrium is reached. No damage can occur to the intact rock. The explicit fractures only can shear or slip.

At the end of both modeling steps, the stress field is sampled on the explicit and the implicit fractures to compute the average normal stress per fracture, for the entire DFN. For explicit fractures, the stresses are directly extracted from the 3DEC model mesh. For implicit fractures, which are not meshed, an average stress tensor is calculated at regularly spaced points on the fracture plane. Stress computations exclude fracture surface fractions located in the excavated volume. The stresses are exported to DFN.lab, as input to the definition of the fracture transmissivities (eq 1).

## 3.2 Hydrogeological model

The definition of the equivalent hydraulic conductivity in the vicinity of the excavation depends both on the transmissivities of the open fractures, and on the presence of a set of interconnected fractures forming a connected cluster between active hydraulic boundaries (open connected DFN). If no connected path of transmissive fractures exists, the equivalent conductivity is simply zero.A rock mass hydraulic conductivity can be calculated from the fluid flow passing through a surface, under given head gradient conditions. In the present case, the shape of the volume around the measuring surface is a cylindrical and thick ring (Figure 2) whose central axis is the axis of the tunnel itself. The thickness of the domain is equal to $r_1 - r_0$, where $r_0$ is the tunnel radius and $r_1$ the domain outer edge radius. Its height is equal to the one of the tunnel (noted $L$). Fixed hydraulic heads, $h_0$ and $h_1$, are set at the domain inner and outer surfaces, respectively; no flow are set on the two remaining surfaces (front and back of the domain). This creates a radial head gradient directed toward the tunnel (Figure 2). If the DFN creates a connected path, a steady-state fluid flow simulation is done with DFN.lab, and the flow rate $Q$ is derived. The equivalent hydraulic conductivity ($K$) of the fracture network is calculated using Dupuit's formula for radial flow (eq. 3):

$$K = \frac{\ln(r_0/r_1)}{2\pi L(h_1 - h_0)} \cdot Q \tag{3}$$

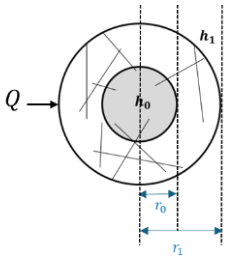


Figure 2. Schematic representation in 2D of the hydraulic boundary conditions setup. The cylindrical domain with radius $r_1$ and $r_0$. Fixed heads ($h_0$ and $h_1$) are imposed on the tunnel walls and the outer model boundary.

Note that one could keep the same volume around the tunnel and change the hydraulic boundary conditions by inverting them, i.e. no flow on the radial faces and loads on the front and back faces. In both cases the connectivity of the DFN to the hydraulically active boundaries is a necessary condition for defining hydraulic conductivity. If no fractures form a connected cluster between the two active boundaries, there will be no flow in the system.

# 4 Results

## 4.1 Connectivity in the DFN model

Figure 3a shows one realization of the Open-DFN model (defined in Section 2). The connected cluster DFN (Figure 3b) is computed between the tunnel and the domain faces orthogonal to the x- and z-directions. It visibly contains much less fractures than the Open DFN and the connected structure depends on the largest fracture connecting the domain alone.

*a)* *b)*

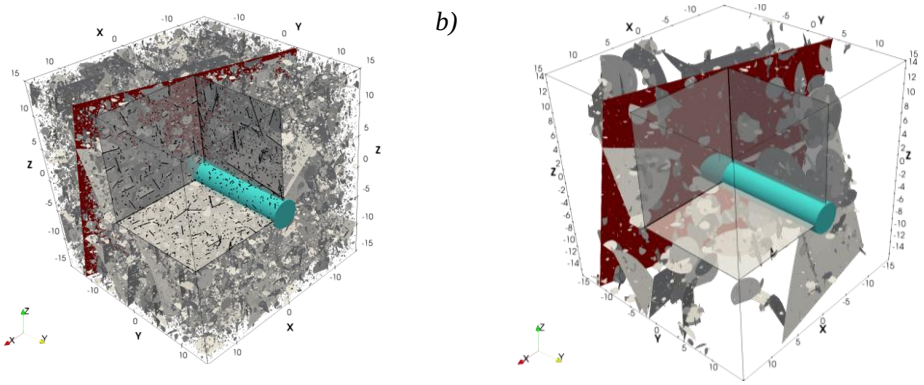

Figure 3. *a)* Realization of the Open DFN model in the domain of size $L$ =30 m around the tunnel (blue color). *b)* Same view after Connected cluster DFN. The largest fracture is highlighted (red color). The faces of the corner cube are used as slices to display fracture traces.

## 4.2 Stress distribution in the vicinity of the excavated tunnel

### 4.2.1 In a homogeneous medium

For a homogeneous and isotropic medium, the stress distribution around a tunnel can be predicted analytically (Jaeger et al., 2007). The normal component of the stress on a plane of given orientation can then be calculated, for any orientation and position relative to the tunnel. This is illustrated in Figure 4, where the evolution of the normal stress with the distance to the tunnel (horizontal direction orthogonal to the tunnel, $x$ axis) is plotted for three orientations relative to the tunnel: transverse (pole along y), tangential (pole along x) and longitudinal (pole along z).

For transverse fracture planes, there is no variation in normal stress with the distance from the tunnel. For tangential fractures, the normal stress tends to zero near the tunnel and rapidly increases with distance, asymptotically approaching $\sigma_h$. For the longitudinal case, the normal stress increases slightly near the tunnel and then decreases with distance, tending toward $\sigma_v$ at larger distances. Beyond five times the size of the tunnel, the induced stress perturbation vanishes.

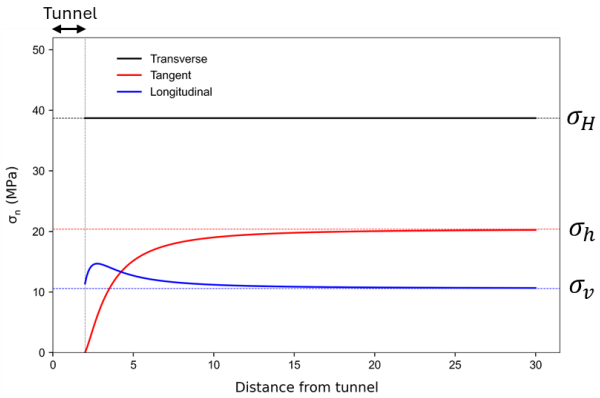


Figure 4. Evolution of the normal stress $\sigma_n$ as a function of the distance to the tunnel for three measuring planes of orientation: transverse (black), tangential (red), longitudinal (blue).

### 4.2.2 With explicit fractures

As mentioned in section 3.1, a limited number of fractures can be explicitly included in the 3DEC model. the DFN is thus divided into two groups: explicit fractures (Figure 5a), which are meshed in the 3DEC model, and implicit fractures (Figure 5b), which are used as measurement locations. For this study, the selection is based on the fracture size, with the ones larger than 3.5 m modelled explicitly, resulting in 47 explicit fractures.

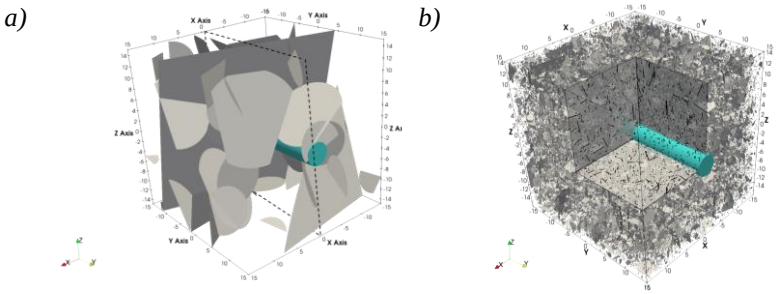


Figure 5. *a)* Explicit and *b)* Implicit fractures in the 3DEC geomechanical model.

Before the tunnel excavation, fractures under remote stress conditions induce stress fluctuations (Figure 6a). Excavating a tunnel triggers additional stress variations near the excavation.

Fracture mean normal stresses are computed for both the explicit and implicit fractures, before and after the tunnel excavation. Note that in each fracture plane there are likely local variations of normal stresses (Figure 6b). The variability in the plane is not analysed further and only the average normal stress is considered for the transmissivities.

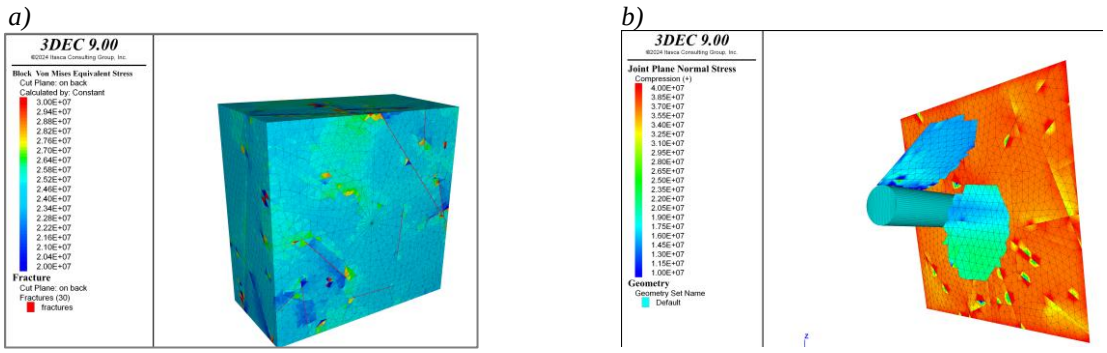


Figure 6 *a)* Von Mises Stresses before the excavation. *b)* Fracture in-plane normal stresses for three selected explicit fractures after the tunnel excavation.

## 4.3 Fracture transmissivities

The transmissivity distribution of the fractures shows minimal variation due to the excavation (Figure 7a). Although individual fractures may experience significant changes in transmissivity (exceeding 100% in some cases), these changes do not appear in the overall distribution. This can be partly attributed to some fractures opposing effects, where transmissivity increases in some fractures while simultaneously decreasing in others (Figure 7b).

Fractures exhibiting strong transmissivity variations are typically smaller and located close to the tunnel, within approximately twice the tunnel radius. Fractures with increased transmissivity are predominantly located on the sides of the tunnel (along the x-direction) and are generally tangentially oriented. In contrast, fractures with decreased transmissivity are mostly located above or below the tunnel (along the z-direction) and are mostly in the longitudinal category.

*a)* *b)*

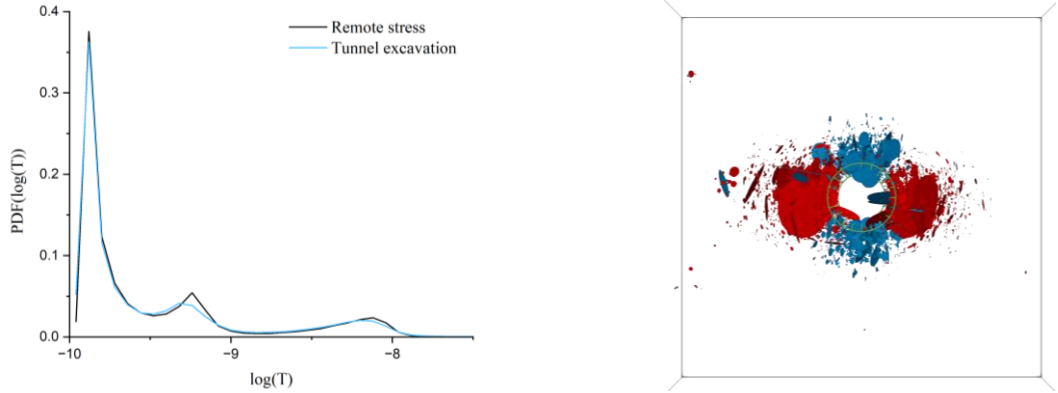


Figure 7. *a)* Distribution of transmissivities before (black) and after excavation (blue). *b)* Fractures with transmissivities increased by at least 50% (red) and decreased by at least 50% (blue) sue to the excavation.

## 4.4 Equivalent hydraulic conductivity

The decrease in hydraulic conductivity with increasing domain size (Figure 8) is visible for the two conditions, before and after excavation. This evolution is typical in fractured rocks below or close to the percolation threshold, where the connected cluster consists of a single main fracture. In the present case, the volume under consideration is atypical in that the longitudinal dimension $L$ is fixed at 30 m, while the outer radius of the ring ($r_1$), and therefore the volume, increases in the transverse direction. When $r_1$ is very small, several connected paths appear, but they are only formed by single fractures. As $r_1$ increases, this connectivity disappears. It should also be noted that in this configuration there is no connected path between the opposite faces of the volume under consideration and no flow path parallel to the tunnel.

The comparison of the results before and after excavation shows no significant difference. If the hydraulic conductivity value is dominated by the transmissivity of the large and connected fracture, then this value did not change after excavation. This result is consistent with the configuration presented, where the hydraulic conductivity value is dominated by the transmissivity of the large and connected fracture that is orthogonal to the maximum horizontal stress.

*a)* *b)* *c)*

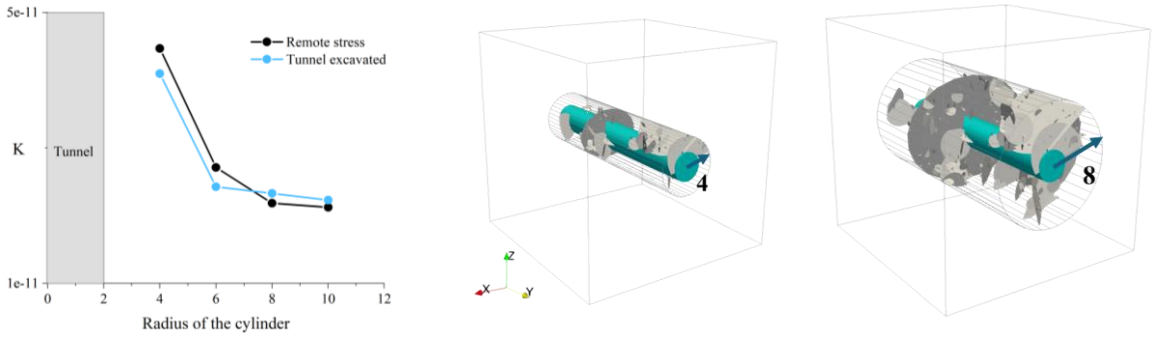


Figure 8. *a)* Variation of the equivalent hydraulic conductivity $K$ with increasing volume (increase of the outer radius $r_1$, see Figure 2). *b)* and *c)* DFN radially connected cluster, for $r_1$ equal to 4 m and 8m, respectively.

# 5 Concluding remarks

In this study we have analyzed the effect of tunnel-induced stress redistribution on the hydromechanical properties of fractured rocks, with a particular emphasis on fracture normal stress, transmissivity and hydraulic conductivity. The developed workflow is general but was used to study only one specific configuration.

With the tested scenario, no significant impact of the tunnel excavation on the hydraulic conductivity has been highlighted. The results showed that hydraulic conductivity, at the scale evaluated, is primarily controlled by the connectivity structure of the DFN and that the transmissivity of the largest fracture was only slightly affected by the tunnel, due to its orientation. The analysis shows that the scale of connectivity of the DFN is greater than the scale of disturbance caused by the tunnel. Under these conditions, although the stress and transmissivity of certain fractures may be affected locally, there is no effect on a larger scale. While the fracture transmissivity can vary up to 100% close to the tunnel, the variation depends on the fracture orientation and relative position to the tunnel. In the studied conditions, the transmissivity can be multiplied by a factor of 1.5 on the sides of the tunnel and divided by the same amount above and below it.

This study will be continued by analyzing different configurations of DFN realizations and models, and by reconsidering several hypotheses: the possibility of reactivating not only of fractures already open, but also of fractures initially sealed; and excavation-induced additional damage. This will potentially increase connectivity and increase the impact of the hydromechanical coupling in the tunnel vicinity.

# 6 References

Darcel, C., Davy, P., Le Goc, R., de Dreuzy, J.R., Bour, O., 2009. Statistical methodology for discrete fracture model-including fracture size, orientation uncertainty together with intensity uncertainty and variability.

Darcel, C., Le Goc, R., Lavoine, E., Davy, P., Mas Ivars, D., Sykes, E., Kasani, H.A., 2024. Coupling stress and transmissivity to define equivalent directional hydraulic conductivity of fractured rocks. Eng. Geol. 342, 107739. https://doi.org/10.1016/j.enggeo.2024.107739

Davy, P., Le Goc, R., Darcel, C., 2013. A model of fracture nucleation, growth and arrest, and consequences for fracture density and scaling. J. Geophys. Res. Solid Earth 118, 1393–1407.

de Dreuzy, J.-R., Davy, P., Bour, O., 2001. Hydraulic properties of two-dimensional random fracture networks following a power law length distribution: 2. Permeability of networks based on lognormal distribution of apertures. Water Resour. Res. 37, 2079–2095. https://doi.org/10.1029/2001WR900010

Fox, A., La Pointe, P., Simeonov, A., Hermanson, J., Oehman, J., 2007. Statistical geological discrete fracture network model. Forsmark modelling stage 2.2.

Itasca, 2024. 3DEC (3 Dimensional Distinct Element Code) v 9.0.

Jaeger, J.C., Cook, N.G.W., Zimmerman, R.W., 2007. Fundamentals of Rock Mechanics. Blackwell, Malden, Mass.

Lavoine, E., Davy, P., Darcel, C., Mas Ivars, D., Kasani, H.A., 2024. Assessing Stress Variability in Fractured Rock Masses with Frictional Properties and Power Law Fracture Size Distributions. Rock Mech. Rock Eng. 57, 2407–2420.

Le Goc, R., Pinier, B., Darcel, C., Lavoine, E., Doolaeghe, D., de Simone, S., De Dreuzy, J.-R., Davy, P., 2019. DFN. lab: software platform for Discrete Fracture Network models., in: AGU Fall Meeting 2019. Agu.

Liu, H.-H., Rutqvist, J., Zhou, Q., Bodvarsson, G.S., 2004. Upscaling of Normal Stress-Permeability Relationships for Fracture Networks Obeying Fractional Levy Motion, in: Elsevier Geo-Engineering Book Series. Elsevier, pp. 263–268. https://doi.org/10.1016/S1571-9960(04)80051-X

Martin, C.D., 2007. Quantifying in situ stress magnitudes and orientations for Forsmark – Forsmark stage 2.2.

Olofsson, I., Simeonov, A., Stephens, M., Follin, S., Nilsson, A.-C., Roeshoff, K., Lindberg, U., Lanaro, F., Fredriksson, A., Persson, L., 2007. Site descriptive modelling Forsmark, stage 2.2. A fracture domain concept as a basis for the statistical modelling of fractures and minor deformation zones, and interdisciplinary coordination.

Selroos, J.-O., Ivars, D.M., Munier, R., Hartley, L., Libby, S., Davy, P., Darcel, C., Trinchero, P., 2022. Methodology for discrete fracture network modelling of the Forsmark site. Part 1 – concepts, data and interpretation methods 261.

Snow, D.T., 1969. Anisotropic permeability of fractured media. Water Resour. Res. 5, 1273–1289. https://doi.org/10.1029/WR005i006p01273

Rutqvist, J., & Stephansson, O. (2003). The role of hydromechanical coupling in fractured rock engineering. *Hydrogeology Journal*, *11*(1), 7-40.

Tsang, C.-F. (2024). Coupled Thermo-Hydro-Mechanical Processes in Fractured Rocks: Some Past Scientific Highlights and Future Research Directions. *Rock Mechanics and Rock Engineering*, *57*(8), 5303-5316. https://doi.org/10.1007/s00603-023-03676-7